Sparse Random Ultrasound Phased Array for Focal Surgery

Stephen A. Goss, *Senior Member, IEEE,* Leon A. Frizzell, *Senior Member, IEEE,* Jeffrey T. Kouzmanoff, Joseph M. Barich, and Jeffrey M. Yang

Abstract— **Ultrasound phased arrays offer several advantages over single focused transducer technology, enabling electronically programmable synthesis of focal size and shape, as well as position. While phased arrays have been employed for medical diagnostic and therapeutic (hyperthermia) applications, there remain fundamental problems associated with their use for surgery. These problems stem largely from the small size of each array element dictated by the wavelength employed at surgical application frequencies (2–4 MHz), the array aperture size required for the desired focal characteristics, and the number of array elements and electronic drive channels required to provide RF energy to the entire array. The present work involves the theoretical and experimental examination of novel ultrasound phased arrays consisting of array elements larger than one wavelength, minimizing the number of elements in an aperture through a combination of geometric focusing, directive beams, and sparse random placement of array elements, for tissue ablation applications. A hexagonally packed array consisting of 108 8-mm-diameter circular elements mounted on a spherical shell was modeled theoretically and a prototype array was constructed to examine the feasibility of sparse random array configurations for focal surgery. A randomly selected subset of elements of the prototype test array (64 of 108 available channels) was driven at 2.1 MHz with a 64-channel digitally controlled RF drive system. The performance of the prototype array was evaluated by comparing field data obtained from theoretical modeling to that obtained experimentally via hydrophone scanning. The results of that comparison, along with total acoustic power measurements, suggest that the use of sparse random phased arrays for focal surgery is feasible, and that the nature of array packing is an important determinant to observed performance.**

I. Introduction

A NUMBER OF recent studies have demonstrated the feasibility of the practical clinical realization of noninvasive surgery using high-intensity focal ultrasound [1]–[4], with other studies in animal models suggesting further future promise for this technology [5]–[8]. Such surgical applications require precise control of the size and location of the focal therapy beam, as well as consideration of the effects of the entrance and exit beams associated with the use of focal fields [9]–[11].

Applications of ultrasound tissue ablation have been largely confined to brain [12], [13], ocular tissues [14], prostate [1], liver [6]–[8], [15], and atherosclerotic tissues [16], though other surgical applications are possible, including the focal ablation of tumors [5], [8], [17]. Breast cancer treatment, for example, can greatly benefit from noninvasive surgical techniques in that 1) early detection frequently results in the identification of small discrete lesions which offer viable ablation targets which can be diagnostically monitored after treatment, 2) current forms of treatment usually require, at a minimum, potentially disfiguring surgery which can be avoided via noninvasive methods, and 3) the thickness, available acoustic window, and intervening tissue properties of the breast suggest that the accessibility of the entire tissue is possible, though precautions to protect the chest wall may be required.

Surgical ultrasound beams have historically been produced by single-element transducers focused geometrically (i.e., spherical shell "bowl" transducers), or with lenses [12]. The acoustic beams produced by such devices are therefore fixed in shape, and in position, with respect to the face of the source transducer. Modification of focal size can be accomplished only by changing the physical properties of the source transducer (i.e., spherical shell aperture or radius of curvature, or lens dimensions or properties). A precisely controlled rapidly translatable mechanical system is therefore required to move the ultrasound focus to the target location(s), however, beam shape is uniquely defined and fixed by the transducer, and is not modified during the course of a procedure.

Phased arrays offer the advantage of not only electronic steering of a focal ultrasound beam to precise target positions without mechanical scanning, but also can provide a means for modifying the characteristics of the ultrasonic surgical beam [18]. Such electronic beam synthesis can be employed to steer the beam to specific target locations, as well as modify the focal area of the array to particular clinical needs [19].

Ultrasound phased arrays have long been employed in diagnostic imaging, and have more recently been developed for experimental therapeutic treatment [18], [20]–[23]. In most applications of the past, an array interelement spacing of $\lambda/2$ (where λ is the acoustic wavelength) has been employed to avoid the problems associated with the production of grating

Manuscript received November 2, 1995; revised May 30, 1996. This work was supported in part by Grant CA66462 from the National Institutes of Health.

S. A. Goss was with Labthermics Technologies, Inc., Champaign, IL 61820 USA. He is now with the University of Illinois, Champaign, IL 61820 USA (e-mail: sa-goss@staff.uiuc.edu).

L. A. Frizzell, J. M. Barich, and J. M. Yang are with the Department of Electrical and Computer Engineering, University of Illinois, Urbana, IL 61801 USA.

J. T. Kouzmanoff is with Labthermics Technologies, Inc., Champaign, IL 61820 USA.

Publisher Item Identifier S 0885-3010(96)07862-8.

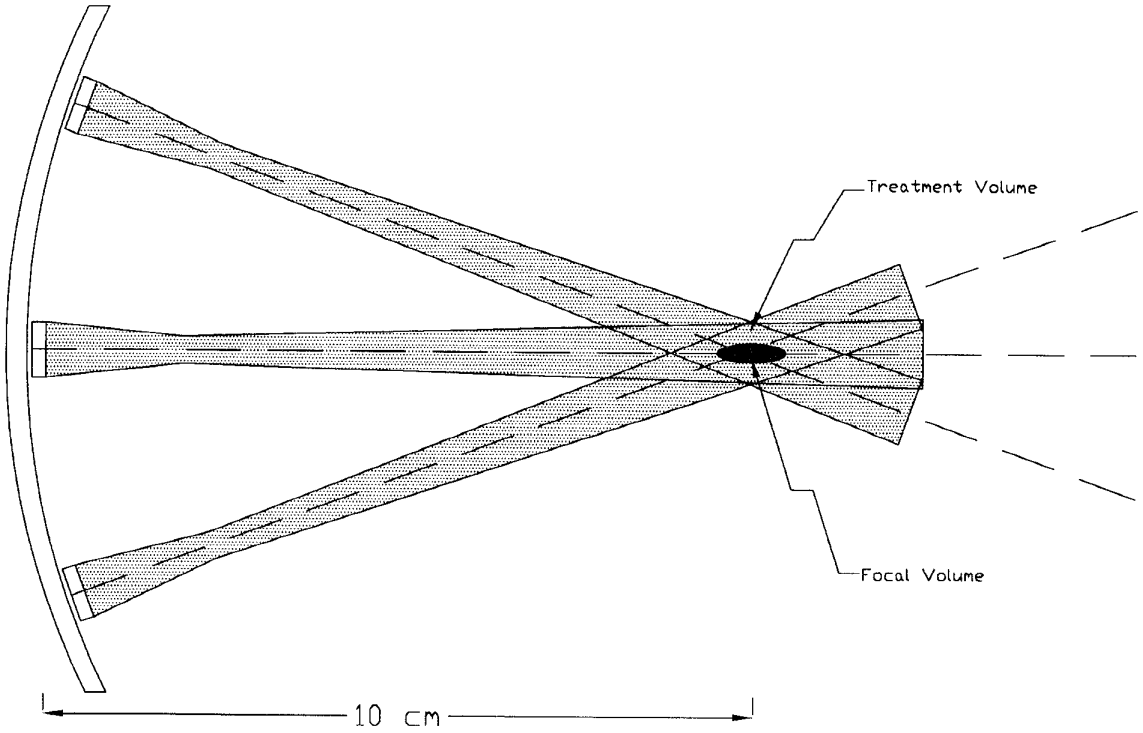

Fig. 1. Two-dimensional illustration of beam overlap in the treatment volume. The illustration shows the 8-mm-diameter sources used in the experimental array and the beamwidth at 10 cm from each source is the calculated quarter-power beamwidth for the 8-mm source. The extent of the treatment volume and the array focus, enlarged for illustration, are shown.

lobes which degrade, or eliminate, proper system performance. At megahertz frequencies, however, the wavelength in water (and tissue) is about $1.5/f$ mm, where f is the frequency in MHz, which limits the array to small apertures for reasonable numbers of array elements. This is less of a problem in imaging, where a small array aperture will produce a desirable elongated focal region, and may provide an advantage for imaging within tight acoustic windows. For therapy, however, a large aperture is generally necessary to develop sufficient intensity gain for heating or tissue ablation, requiring more array elements whose individual size is inversely proportional to the operating frequency. The need to provide separate RF drive and control further confounds the realizability of surgical ultrasound phased arrays, drives up costs, and adds array construction complications which may be prohibitive to commercial development.

This study examines the feasibility of using a sparsely filled spherical ultrasonic phased array for focal surgery to reduce the number of array elements and RF drive channels required for practical implementation. Sparse random arrays have long been used in the design of communication antenna array systems [24]–[26], and very recently, sparse arrays have been investigated for use in ultrasound imaging systems [27], [28]. For the present application, the design concept involves a spherical acoustic aperture, with the focus of the aperture geometrically centered on the target volume when all elements of the array are excited at a common phase. The phase of the signals applied to individual elements in the array are then controlled to move the focal region to ablate the entire tumor volume using a succession of exposures at sites within the tumor. The performance of two different spherical arrays is analyzed to determine their suitability for surgical treatment.

II. Methods

The noninvasive surgical ultrasound array developed in this study consists of circular ultrasonic elements mounted on a spherical shell. With the geometric focus of such an array centered on the volume to be treated (ablated), the focal region of the array can be electronically scanned to treat the entire volume. Since it is desired to minimize the number of array elements, the element size was chosen to be as large as possible while allowing the range of scanning desired. While each element can be directive, its range of useful amplitude must encompass the volume to be treated, since a large amplitude focus can only be generated within the extent of the fields of the individual elements. This is illustrated in two dimensions in Fig. 1. Here, the limited region of overlap of the three beams shown defines the treatment region where the focus can be scanned, and minimizes the possibility of spurious lobes outside the treatment volume.

Theoretical calculations of the field pattern of the entire array were made by first determining the field pattern from one of the circular elements in the array. The results from this calculation were then used to compute the field from the entire array by a superposition of the fields generated by each element, as discussed below.

A. Field Computation for a Single Circular Source

Several computational methods have been used to determine the pressure distribution of a circular source. Possibly the most widely used method, and the method implemented in this study, is the Point Radiator Method (also known as the Point Source Method) which involves representing the acoustic piston source by many point radiators [29]–[31]. The circular source is divided into incremental areas, ΔA, so small that the acoustic pressure field produced by each can be approximated as that resulting from a point (spherically radiating) source positioned at the center of the incremental area. The field from the circular source is the sum of the contribution from each of its incremental areas as follows:

$$p = j\frac{\rho c k U_0 \Delta A}{2\pi} \sum_{\text{Surface}} \frac{e^{-(\alpha + jk)R}}{R}. \tag{1}$$

Here, p is the pressure, ρ is the density of the medium, c is the speed of sound in the medium, k is the propagation constant, U_0 is the velocity amplitude of the surface of the source, R is the distance from the center of an incremental element to the point where the field is calculated, and α is the attenuation coefficient (which is taken as zero to approximate that of water in the results presented here). The Point Radiator Method is only valid if the dimensions of the incremental area are small compared to a wavelength. Thus, the spacing between the point radiators was chosen as one-sixth of a wavelength, which is typically small enough to give an accurate representation of the field. In this study the incremental areas were chosen to be squares so that they would lie in an easily referenced square grid.

The acoustic pressure field of the circular source, because of its symmetry, is completely defined by computing the pressure amplitude as a function of distance from the source, z, and distance off the axis, r. The acoustic pressure field was calculated, using a Dell 466/M personal computer with programs written in C++ (Microsoft Visual C++), for sources of several different sizes, relative to a wavelength, and found to be in excellent agreement with the fields reported by Zemanek [29] for sources of the same size.

The pressure field distribution (magnitude and phase) for all r–z combinations in the range of interest ($r \leq 50$ mm; 50 mm $\leq z \leq$ 150 mm; where r is the perpendicular distance from the point in the field to the axis of the source and z is the corresponding distance along the axis from the source) was computed for a single circular 8-mm-diameter source radiating into a semi-infinite water medium. These data were stored in a lookup table (600 samples in the r direction by 1000 samples in the z direction) for use in computing the field for the spherical array.

B. Field of the Spherical Array

The combined field from arrays of such circular sources mounted on a spherical shell was calculated through summation of the pressure contribution from each source in the array at each point in the resultant field. This contribution was determined for each source by calculating the location of the field point in terms of both its distance along the axis from the particular source and its distance off the source axis, and using a linear interpolation from the nearest four points in the lookup table to calculate separately the values of the pressure magnitude and phase at the point. The relative magnitude and phase for each source can be adjusted, by changing the values in its lookup table, to provide either shading or steering, respectively, for the spherical array. When the surface velocity of each element was in phase, the focus of the spherical array occurred at the geometric focus. To steer the focus to a new point the distance from that point to each source was calculated and the phase adjusted so that each source provided a pressure contribution in phase with all other sources at the desired focal point. The field was calculated at a density of five points per millimeter in all directions.

C. Experimental Hexagonal Array Construction

An experimental array was constructed using 108 individual PZT-8 piezoceramic transducers 8 mm in diameter with a one-half wavelength thickness of 1 mm for a resonance frequency of 2.1 MHz. Each transducer was mounted in a special cylindrical housing, which was in turn mounted in holes drilled in a stainless steel spherical support shell. Each circular array element was mounted on the front (concave) surface of the spherical shell such that the active face of the transducers defined a sphere with a diameter (aperture) of approximately 100 mm and a radius of curvature of approximately 102 mm. Electrical connection to the positive electrode of each transducer was made via a spring contact at the back of each source which was connected to cables feeding from a distribution box connected to 64 digitally controlled RF amplifiers. In this experimental implementation, no electrical impedance matching between the amplifiers and the transducers was provided. The front face of each transducer was connected to the grounded housing with conducting epoxy (Tra-Con, Inc.). For purposes of demonstration, the experimental array constructed during this study had the sources mounted in a hexagonal pattern on the spherical shell. Such a hexagonal pattern provides the maximum number of source positions on the face of the shell. A drawing of the hexagonal array identifying those elements excited for the theoretical computations and experimental measurements reported under results is shown in Fig. 2.

D. Multichannel RF Drive and Phase Control System

The electronics to drive each element of the test array consisted of 64 channels with independently controllable RF amplitude and phase. The RF amplifier control is a two-channel Class E amplifier with each channel preceded by an independent programmable linear regulator. Each channel also has an rms current sense amplifier, overcurrent protection circuitry, overcurrent status bit, and a D/A–A/D

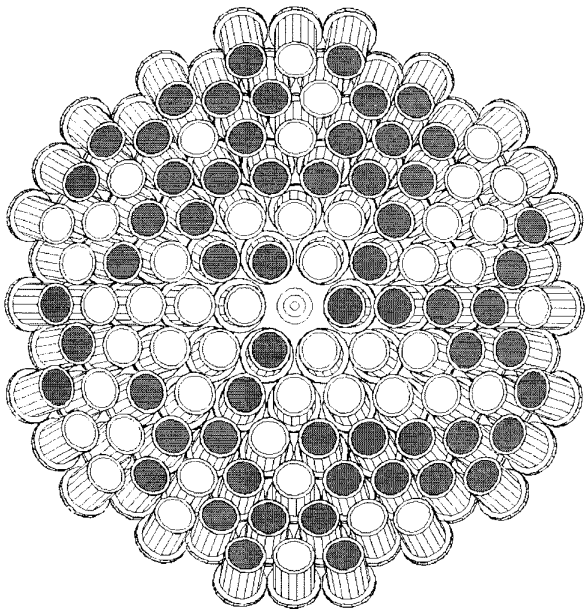

Fig. 2. Three-dimensional drawing of the hexagonal array showing the 64 transducers (filled gray) of the 108 total that were excited for the theoretical and experimental fields presented.

diagnostic readback system. Phase is controlled in 22.5° increments, which has been shown in previous studies to provide adequate phase resolution over the range from 0 to 360° [32]. Each amplifier can deliver approximately 40 W of RF power into 50 Ω. User control of the phased array originates from amplitude and phase data sent to the hardware to synthesize a particular field. The field can consist of one or more focal regions. The user can also control multiple fields which are applied sequentially to the hardware to realize scanned "paths" of energy deposition.

Control of the phased array is accomplished through two layers of software, a higher layer running on a 386-based PC and a lower layer running on an 8031 microcontroller card. The user makes control requests via the PC keyboard, and the request is handled by the PC and sent via a serial interface to the 8031 card. The 8031 card stores this information in its own memory so that the PC needs only to send modifications. The 8031 then programs the individual components of amplitude and phase control sequentially to fulfill the request of the user. Each field is left in place for a user-specified duration. A digital interface card implemented in CMOS technology links the backplane of all 64 amplifier channels (32 two-channel amplifier boards) with the 8031 microcontroller, and performs address decoding, read/write cycle timing, and data transceiving functions.

E. Acoustic Field Measurements

Acoustic field plots of the prototype array were obtained using a computerized positioning and data acquisition system capable of moving and recording the output of a small acoustic hydrophone over three orthogonal dimensions with respect to the ultrasonic applicator. The hydrophone was precisely moved to known positions with respect to the face of the ultrasound applicator to measure the local acoustic field pressure as a function of spatial position, with the relative acoustic pressure amplitude and the position of each amplitude measurement recorded by the data acquisition system. All measurements were performed in degassed water. The positioning system employs three precision lead screw mechanical slide assemblies (Velmex, Inc.) having hard anodized dovetail ways, with each having absolute positional repeatability of better than ±0.051 mm. Acoustic pressure was measured with a small needle wide-band hydrophone probe (Dapco Model NP-10-1) having an active element diameter of 0.635 mm. The probe, mounted on the three-dimensional (3-D) positioning system, is polled by the data acquisition system every 0.0127 mm. Every 32 individual data points are averaged and displayed on a computer monitor, such that a value for acoustic pressure is displayed every 0.406 mm. Thus, for a 20 cm scan, 492 data points, each representing the average of 32 measurements, are displayed.

The scan coordinate system is defined by xy being the transverse scan plane parallel to the face of the applicator, and z perpendicular to this plane serving to define the range away from the applicator surface. Transverse plots were performed along the y direction, with x and z held constant. Many of these linear plots, at different values of x, were combined by the data acquisition software to display the two-dimensional (2-D) spatial variation of the acoustic pressure distribution (or the square of the pressure to get a quantity proportional to intensity) in a transverse plane.

F. Total Acoustic Power Measurements

Total acoustic power, including the power in all grating lobes, was determined by measuring the force on an absorbing target. The force was converted to total acoustic power using the relation 1 W = 67 mg [33]. The transducer array was submersed in a small tank filled with degassed water, with a neoprene rubber absorber in the bottom, set on the top of an electronic balance (Sartorius Model U6100). The total acoustic power was measured as a function of the total dc power applied to the RF drive system.

III. Numerical and Experimental Results

Results are presented for two different arrays. Both theoretical and measured fields are presented for the 108-element hexagonal array described above, where a subset of 64 randomly selected elements is excited to mimic a sparsely filled condition. Theoretical results are also presented for another array, hereafter referred to as the random array, with 64 elements randomly located on a spherical surface of the same dimensions as for the hexagonal array. The random selection of elements excited for the hexagonal array, and the random locations of elements for the random array, were determined using a pseudorandom selection by computer.

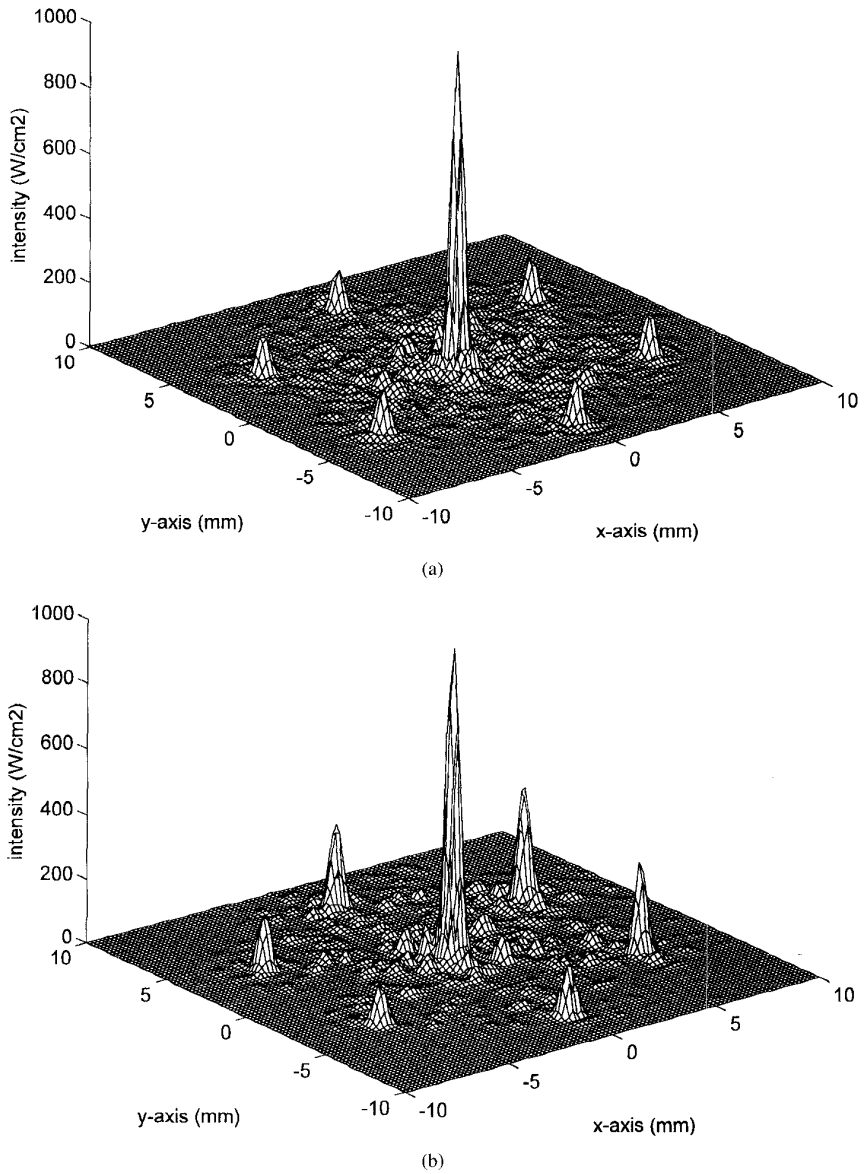

Fig. 3. Relative intensity versus x and y at a distance of 10 cm from the hexagonal array with no steering of the focus: (a) theoretical and (b) measured. The intensity shown for the theoretical plot assumes an intensity at the face of the source of approximately 0.77 W/cm^2. The intensity at the focus for the measured plot was normalized to that of the theoretical plot.

A. Hexagonal Array

The spherical segment array with elements arranged in a hexagonal pattern was examined both theoretically and experimentally. The theoretical model and experimental system consisted of 108 elements of which only 64 randomly chosen elements were excited at a time. Figs. 3 and 4 show comparisons between the computed field and measured field from a representative selection of 64 elements excited. Fig. 3(a) and (b) shows calculated and measured intensity plots in x and y at a distance $z = 10$ cm from the source, i.e., a transverse plot at the focal distance, with no steering. For these and following plots, the calculated intensity profiles used a source velocity amplitude of 0.1 m/s (corresponding to an intensity at the source of approximately 0.77 W/cm^2), and the measured intensity profiles were normalized so that the peak focal intensity matches that in the theoretical profile (962 W/cm^2). It is readily seen that there are six grating lobes which appear, at significant amplitude with respect to the focus, in both the theoretical and experimental plots. There is excellent agreement between theory and experiment as to the location of these lobes. These six grating lobes were present in all theoretical plots computed, independent of the particular 64 elements selected for excitation. Fig. 4(a) and (b) shows similar plots when the focus is steered 5 mm in the negative y direction. It is readily seen in both figures that the focus decreases in amplitude as it is steered away from the array's geometric center and the grating lobes trailing the focus increase in amplitude, equaling or exceeding that at the focus.

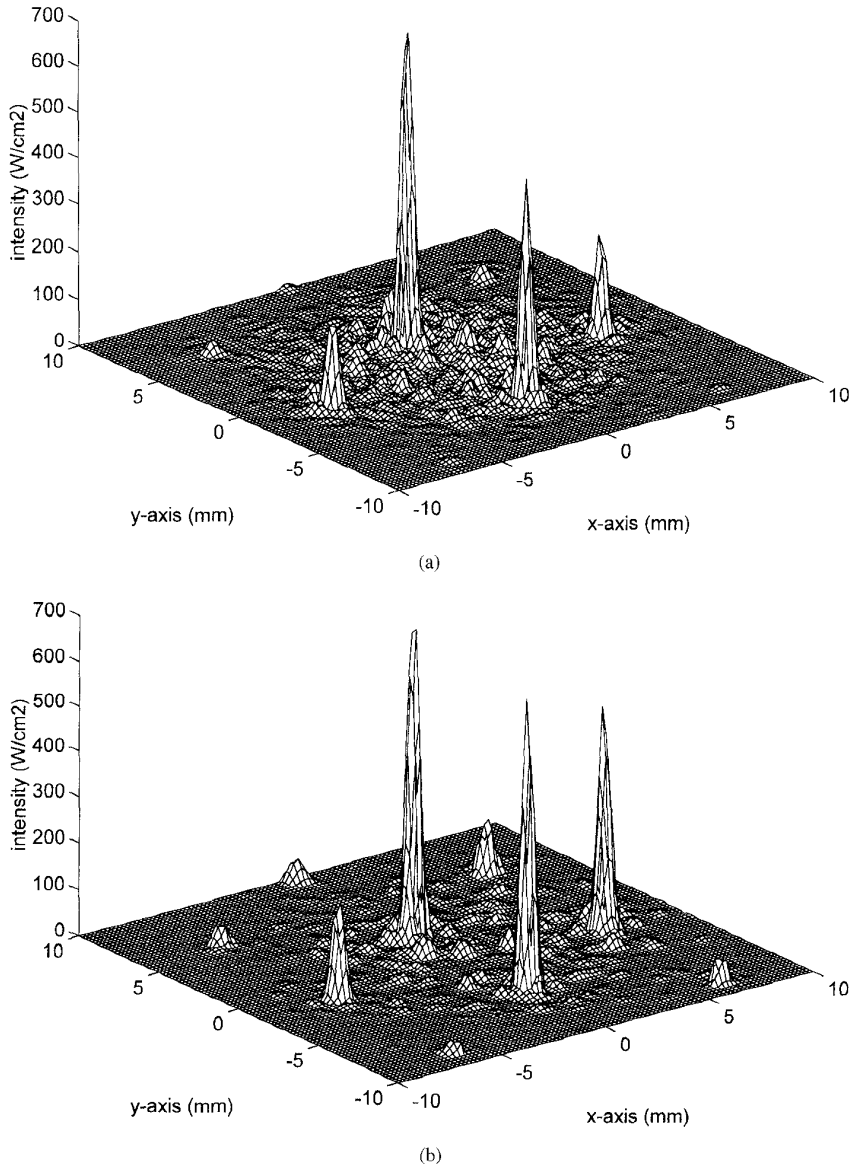

Fig. 4. Relative intensity versus x and y at a distance of 10 cm from the hexagonal array with the focus steered 5 mm in the negative y direction: (a) theoretical and (b) measured. The intensity shown for the theoretical plot assumes an intensity at the face of the source of approximately 0.77 W/cm^2. The intensity at the focus for the measured plot was normalized to that of the theoretical plot.

Fig. 5 shows the intensity profile following along the y axis in the plots from Fig. 3. This figure shows more clearly the excellent agreement between theoretical and experimental intensity profiles, particularly in their location. The half power beamwidth of the focus is observed to be approximately 0.5 mm. It should be noted that, because of errors in the exact placement of the elements, it was necessary to adjust the phase of the signal on each element in the experimental array to produce the appropriate focus for the zero steering condition. Once these phase adjustments were made, they served as the zero phase condition when steering off-axis. However, no compensation was made in the experimental array for variations in transducer output, which likely accounts for the difference in amplitude observed for the grating lobes in the experimental results.

The total acoustic power emitted by the hexagonal array was measured as a function of the applied dc power (see Fig. 6). The plot is very linear up to at least 200 W of applied dc power. The intercept is not zero because it is necessary to reach a threshold dc supply voltage (power) before RF power is supplied to the elements. Beyond that threshold power the results are quite linear. The overall efficiency of the array and amplifiers, with no electrical matching between the amplifiers and transducer elements, was less than 30%.

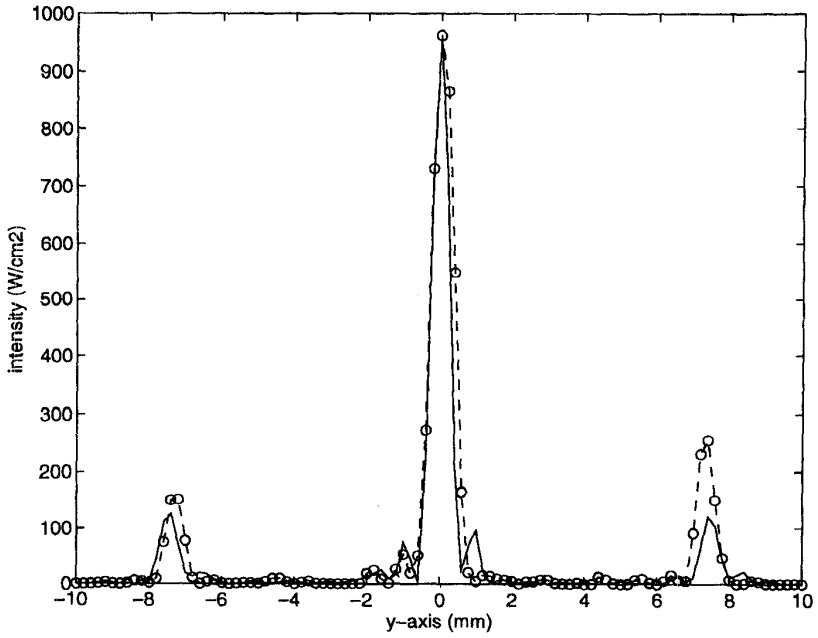

Fig. 5. Relative intensity along the y axis at 10 cm from the hexagonal array: (solid line) theoretical and (dashed line with datum points) measured. The intensity shown for the theoretical plot assumes an intensity at the face of the source of approximately 0.77 W/cm^2. The intensity at the focus for the measured plot was normalized to that of the theoretical plot.

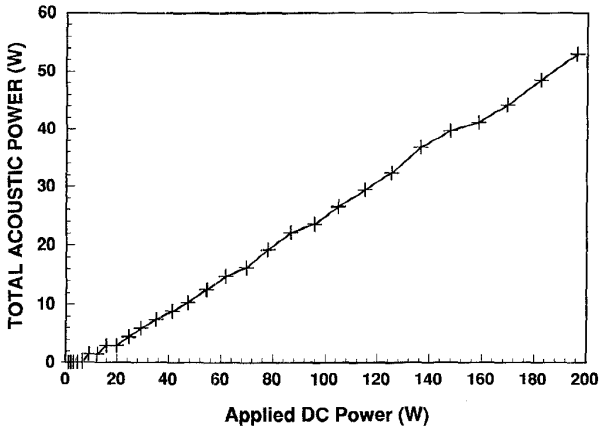

Fig. 6. Measured total acoustic power versus the applied dc power.

In order to determine if sufficient power to produce lesions could be provided by such a sparsely populated array, test lesions in a plexiglass block placed at the focal plane were attempted. An applied dc power of 200 W for 4 s was sufficient to produce lesions not only at the focus, but at the six grating lobes as well. This suggests that the intensity at the focus was well above the lesion threshold for plastic at 2.1 MHz and should be sufficient to produce lesions in tissue.

B. Random Array

Another array was examined theoretically as a means of eliminating the unacceptable grating lobes observed during the theoretical and experimental examination of the hexagonal array. Sixty-four circular 8-mm-diameter sources were randomly distributed on the surface of a sphere having the same dimensions as the hexagonal array, under the constraint that the elements did not overlap. Theoretical plots of the fields for a representative example of a random array yielded very different results with respect to grating lobes. Fig. 7(a) shows a 2-D plot of the intensity in the x–y plane through the focal region transverse to the axis of the array with no steering. Note that the grating lobes which appeared when using an array with regularly spaced elements, the hexagonal array [see Fig. 3(a)], do not appear in this field pattern. The field has an excellent high-intensity focal region with no significant grating lobes. Further, when this beam is steered 2.5 and 5 mm off axis, Fig. 7(b) and (c), there are still no significant grating lobes observed.

IV. Discussion and Conclusion

The theoretical examination of the hexagonal sparsely filled array presented in this study identified the presence of significant grating lobes regardless of the particular subset of 64 elements excited. The presence of such undesirable grating lobes was confirmed experimentally for one representative array of randomly activated elements. The unexpected formation of these grating lobes appears to be due to the regular arrangement of parallel rows of array elements, characteristic of a hexagonal pattern, that produce grating lobes in the form of planes parallel to each of the rows. These planes overlap to produce the six unacceptably large grating lobes in the field of the hexagonal array, even if the rows are not entirely filled. If an intensity above the lesion theshold is chosen for the main beam when steered 5 mm off the geometric focus, one grating lobe is of larger amplitude than the focus and will produce a lesion at the site of the grating lobe. It is clear that the presence of these grating lobes degrades the performance of the hexagonal array and results in a beam pattern that is inadequate for

(a)

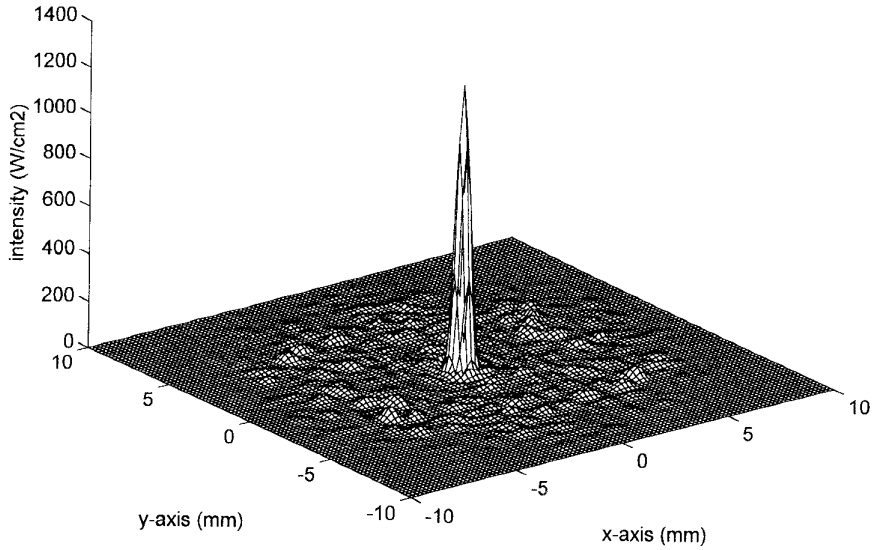

(b)

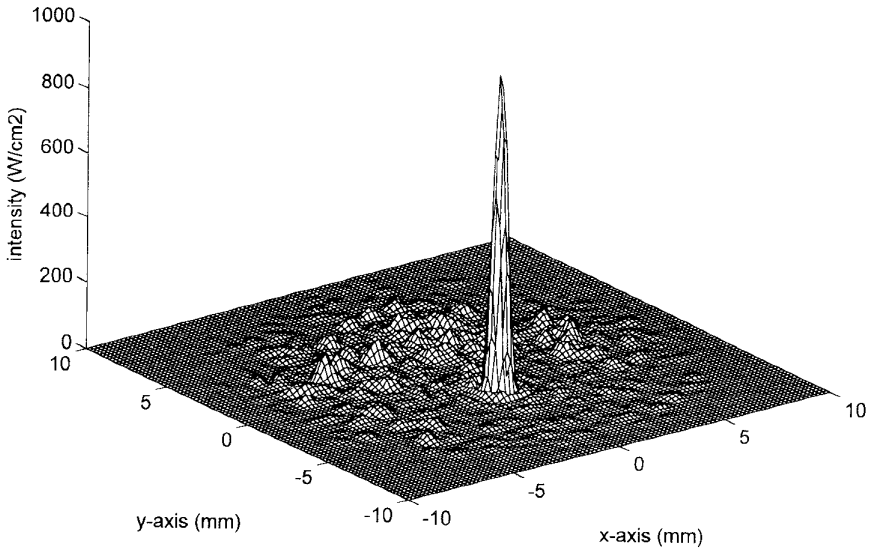

(c)

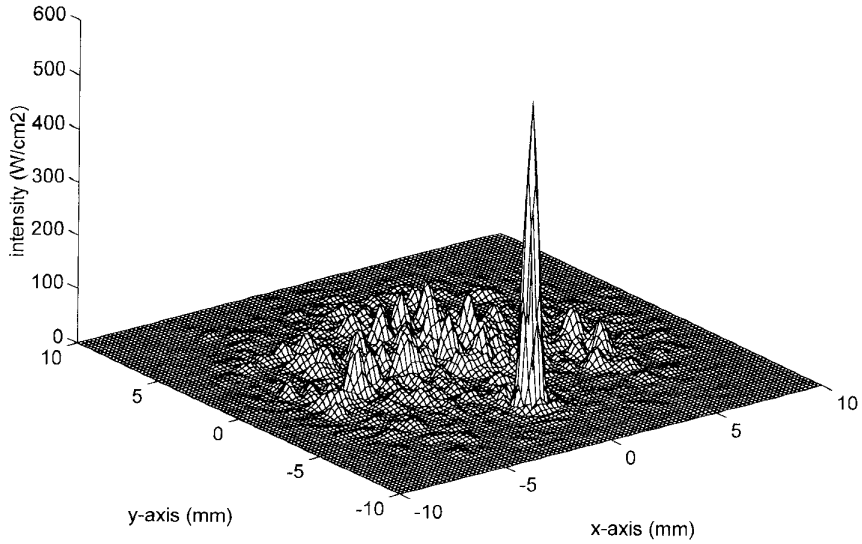

Fig. 7. Theoretical results for relative intensity versus x and y at a distance of 10 cm from the random array with the focus steered (a) 0, (b) 2.5 mm, and (c) 5 mm in the negative y direction.

surgical treatment which involves steering of the focus. It is desirable to have the intensity for any of the grating lobes on the order of 10 dB lower than the intensity at the focus for the full range of beam steering, so that surgical treatment can be well controlled, with no spurious heating of normal tissues.

In order to more fully investigate the origin of the unacceptable grating lobes observed during the theoretical and experimental examination of the hexagonal array, another array was examined theoretically. This array was constructed in exactly the same manner as the hexagonal array, with the important exception that each array element was randomly positioned on the spherical shell. Such an arrangement eliminates the ordered rows of elements of the hexagonal pattern hypothesized to be the source of the grating lobes previously observed. The results of the theoretical analysis of this truly random array showed very low amplitude grating lobes with no steering (approximately 14 dB lower than the peak focal intensity) which increased to approximately 8 dB lower than the peak focal intensity for steering of 5 mm, but were within acceptable limits for the designed steering range of ± 5 mm. For purposes of this study, the steering range has been defined as that for which the intensity at the focus is within 3 dB of the unsteered peak focal intensity and the grating lobes are approximately 10 dB below the peak focal intensity throughout the entire range. Thus, the random array examined theoretically in this study should work well for treating regions 1 cm or less in diameter. It is clear that the random placement of the elements yields an array configuration that produces fields without significant grating lobes that may provide the desired performance for surgical applications. Further, the use of spherical geometry and random, asymmetric location of elements minimizes grating lobes even when array element dimensions and spacing exceed λ.

There are, of course, many other questions that remain concerning the potential utility of such arrays for surgical ablation applications. For example, the degree of sparseness that can be tolerated in the face of the need to form an intense well-behaved beam with steering capability has not been fully investigated. It is also important to distribute sources randomly over the entire array to maintain the full aperture and its associated focal dimensions. The present study suggests that filling the 10-cm aperture spherical shell to approximately 50% of the available active area does not seriously degrade the ability to obtain a sharp focus at intensity levels sufficient to ablate tissue at 2.1 MHz. An increase in sparseness (a decrease in area of sources excited) will decrease the intensity gain of the array, defined as the ratio of intensity at the focus to average intensity at the surface of the sources. Of course, the choice of the size of each array element also affects the performance of the array and the degree of sparseness that can be achieved. The size of elements used in this study (8-mm diameter) limits the distance that the focus can be steered, and consequently the size of the region that can be treated to approximately 1 cm in diameter, but shows that this approach works well. Larger steering distances and treatment volumes are possible, simply by decreasing the element size so that the elements are less directive. This, in turn, results in less power from each element for a given applied voltage. Thus, for a constant aperture size, either the applied voltage must be increased to compensate, within limits that maintain reliability, or the number of elements must be increased, or both. For some applications it may be desirable to treat regions as large as 2–3 cm in diameter. The feasibility of using random arrays for treating these larger tumors is currently being investigated.

Another question that might be asked is how nonlinear effects might differ for a sparse array as compared to a filled aperture spherical source. Since the area of the sources in a sparse array is smaller, the gain is reduced and the sound amplitude must be greater at the surface of each source. Thus, the nonlinear effects would be expected to increase. Ultimately, the role of nonlinear propagation needs to be determined either theoretically or experimentally, but it would seem that as long as the arrays are not made very sparse there would be only slight differences from nonlinear effects observed for other focused surgical systems.

This study has demonstrated that spherical segment phased arrays using large (greater than λ) directive elements randomly spaced on the array surface can provide fields that are free of undesirable grating lobes while providing the necessary power to ablate tissue. Such systems offer the advantages of electronic steering of the focal region without moving the transducer assembly. In addition, the focus can be modified electronically to produce a larger focus if desired. These types of phased array systems offer great flexibility for treating tissues in various locations with widely varying volumes. The strongly focused field produced by a large aperture array can be used when it is critical to avoid damage to nearby structures. However, the focus can be modified to make it larger to facilitate the efficient ablation of large volumes. The development of sparse random array technology may greatly contribute to the improvement and expanded use of noninvasive ultrasound surgical techniques.

ACKNOWLEDGMENT

The authors are indebted to D. Blight for his help fabricating the experimental arrays used in this study.

REFERENCES

[1] R. S. Foster, R. Bihrle, N. T. Sanghvi, F. J. Fry, and J. P. Donohue, "High-intensity focused ultrasound in the treatment of prostatic disease," *Eur. Urology*, vol. 23, no. S1, pp. 29–33, 1993.

[2] R. H. Silverman, B. Vogelsang, M. J. Rondeau, and D. J. Coleman, "Therapeutic ultrasound for the treatment of glaucoma: Results of a multicenter clinical trial," *Amer. J. Ophthalmol.*, vol. 111, pp. 327–337, 1991.

[3] R. J. Siegel, D. C. Cumberland, R. K. Myler, and T. A. DonMichael, "Percutaneous ultrasonic angioplasty: Initial clinical experience," *Lancet*, pp. 772–774, Sept. 30, 1989.

[4] K. Hynynen, A. Darkazanli, E. Unger, and J. F. Schenk, "MRI-guided noninvasive ultrasound surgery," *Med. Phys.*, vol. 20, no. 1, pp. 107–115, 1993.

[5] S. A. Goss and F. J. Fry, "High intensity ultrasonic treatment of tumors," *IEEE Trans. Sonics Ultrason.*, vol. SU-31, pp. 491–496, 1984.

[6] G. ter-Haar, D. Sinnett, and I. Rivens, "High intensity focused ultrasound: A surgical technique for the treatment of discrete liver tumors," *Phys. Med. Biol.*, vol. 34, pp. 1743–1750, 1989.

[7] G. ter-Haar, I. Rivens, L. Chen, and S. Riddler, "High intensity focused ultrasound for the treatment of rat tumors," *Phys. Med. Biol.*, vol. 36, pp. 1495–1501, 1991.

[8] R. Yang, C. R. Reilly, F. J. Rescorla, P. R. Faught, N. T. Sanghvi, F. J. Fry, T. D. Franklin, Jr., L. Lumeng, and J. L. Grosfeld, "High-intensity

focused ultrasound in the treatment of experimental liver cancer," *Arch. Surgery*, vol. 126, pp. 1002–1010, 1991.
[9] R. L. Johnston and F. Dunn, "Ultrasonic absorbed dose, dose rate, and produced lesion volume," *Ultrason.*, vol. 14, pp. 153–155, 1976.
[10] R. C. Robinson and P. P. Lele, "An analysis of lesion development in the brain and in plastics by high-intensity focused ultrasound at low-megahertz frequencies," *J. Acoust. Soc. Amer.*, vol. 51, pp. 1333–1351, 1972.
[11] L. A. Frizzell, C. A. Linke, E. L. Carstensen, and C. W. Fridd, "Thresholds for focal ultrasonic lesions in rabbit kidney, liver, and testicle," *IEEE Trans. Biomed. Eng.*, vol. BME-24, pp. 393–396, 1977.
[12] F. J. Fry, "Intense focused ultrasound: Its production, effects, and utilization," in *Ultrasound: Its Application in Medicine and Biology*, Part II, F. J. Fry, Ed. New York: Elsevier, 1978, pp. 689–736.
[13] F. J. Fry, S. A. Goss, and J. T. Patrick, "Transkull focal lesions in cat brain produced by ultrasound," *J. Neurosurgery*, vol. 54, pp. 659–663, 1981.
[14] F. L. Lizzi, D. J. Coleman, J. Driller, L. A. Franzen, and F. A. Jakobiec, "Experimental, ultrasonically induced lesions in the retina, choroid, and sclera," *Invest. Ophthalmol. Visual Sci.*, vol. 17, pp. 350–360, 1978.
[15] L. A. Frizzell, "Threshold dosages for damage to mammalian liver by high intensity focused ultrasound," *IEEE Trans. Ultrason., Ferroelect., Freq. Contr.*, vol. 35, pp. 578–581, 1988.
[16] A. Ernst, E. A. Schenk, S. M. Gracewski, T. J. Woodlock, F. G. Murant, H. Alliger, and R. S. Meltzer, "Ability of high-intensity ultrasound to ablate human atherosclerotic plaques and minimize debris size," *Amer. J. Cardiology*, vol. 68, pp. 242–246, 1991.
[17] F. J. Fry and L. K. Johnson, "Tumor irradiation with intense ultrasound," *Ultrasound Med. Biol.*, vol. 4, pp. 337–341, 1978.
[18] E. S. Ebbini and C. A. Cain, "Experimental evaluation of a prototype cylindrical section ultrasound hyperthermia phased array applicator," *IEEE Trans. Ultrason., Ferroelect., Freq. Contr.*, vol. 38, pp. 510–520, 1991.
[19] S. A. Goss, "Stationary and phased arrays for ultrasound hyperthermia applicators," in *Hyperthermic Oncology*, vol. 2, T. Sugahara and M. Saito, Eds. New York: Taylor and Francis, 1988, pp. 670–673.
[20] L. A. Frizzell and S. A. Goss, "A 64 element ultrasonic tapered phased array for hyperthermia," in *Proc. 9th Annu. Conf. IEEE Eng. Med. Biol. Soc.*, Boston, MA, Nov. 13–16, 1987, pp. 1642–1643.
[21] L. A. Frizzell, P. J. Benkeser, K. B. Ocheltree, and C. A. Cain, "Ultrasound phased arrays for hyperthermia treatment," in *1985 IEEE Ultrasonics Symp. Proc.*, pp. 930–935.
[22] J. Y. Chapelon, P. Faure, M. Plantier, D. Cathignol, R. Souchon, F. Gorry, and A. Gelet, "The feasibility of tissue ablation using high intensity electronically focused ultrasound," in *Proc. 1993 IEEE Ultrasonics Symp.*, pp. 1211–1214.
[23] X. Fan and K. Hynynen, "Control of the necrosed tissue volume during noninvasive ultrasound surgery using a 16-element phased array," *Med. Phys.*, vol. 22, pp. 297–306, 1994.
[24] Y. T. Lo, "A mathematical theory of antenna arrays with randomly placed elements," *IEEE Trans. Antennas Propagat.*, vol. AP-12, pp. 257–268, 1964.
[25] Y. T. Lo and R. J. Simcoe, "An experiment on antenna arrays with randomly spaced elements," *IEEE Trans. Antennas Propagat.*, vol. AP-15, pp. 231–235, 1967.
[26] A. Ishimaru and Y. S. Chen, "Thinning and broadbanding antenna arrays by unequal spacing," *IEEE Trans. Antennas Propagat.*, vol. AP-13, pp. 34–42, 1965.
[27] G. R. Lockwood, P.-C. Li, M. O'Donnell, and F. S. Foster, "Optimizing the radiation pattern of sparse periodic linear arrays," *IEEE Trans. Ultrason., Ferroelect., Freq. Contr.*, vol. 43, pp. 7–14, 1996.
[28] G. R. Lockwood and F. S. Foster, "Optimizing the radiation pattern of sparse periodic two-dimensional arrays," *IEEE Trans. Ultrason., Ferroelect., Freq. Contr.*, vol. 43, pp. 15–19, 1996.
[29] J. Zemanek, "Beam behavior within the nearfield of the vibrating piston," *J. Acoust. Soc. Amer.*, vol. 49, pp. 181–191, 1970.
[30] D. A. Hutchins, H. D. Mair, P. A. Puhach, and A. J. Osei, "Continuous-wave pressure fields of ultrasonic transducers," *J. Acoust. Soc. Amer.*, vol. 18, pp. 1–12, 1986.
[31] K. B. Ocheltree and L. A. Frizzell, "Sound field calculation for rectangular sources," *IEEE Trans. Ultrason., Ferroelect., Freq. Contr.*, vol. 36, pp. 242–248, 1989.
[32] S. A. Goss, "Tapered linear phased array for ultrasound hyperthermia," Final Tech. Rep. Federal SBIR Grant CA44079, Jan. 20, 1993.
[33] G. Kossoff, "Radiation force," Session 4:1 in *Interaction of Ultrasound and Biological Tissues Workshop Proceedings*, J. M. Reid and M. R. Sikov, Eds. in *Proc. Wkshp. Seattle*, Nov. 8–11, 1971, U.S. Dep. Health Educ. Welfare, Sept. 1972, pp. 159–161.

Stephen A. Goss (S'72–M'78–SM'80) was born on November 21, 1949 in Chicago, IL. He received the B.S., M.S., and Ph.D. degrees in electrical engineering from the University of Illinois at Urbana-Champaign, in 1972, 1974, and 1978, respectively.

From 1978 to 1983 he was a Research Scientist at the Indianapolis Center for Advanced Research, Inc., where he worked in ultrasound biophysics, dosimetry, and cancer therapy, and in the medical applications of ultrasound. He was also an Assistant Professor of Radiology at the Indiana University School of Medicine from 1982 to 1983. From 1983 to 1996, he was Director of Research and Development at URI-Therm-X, Inc., later Labthermics Technologies, Inc., Champaign, IL, where he worked on the development of ultrasound therapy delivery systems for hyperthermia, noninvasive ablation, and associated instrumentation. He presently holds the position of Assistant Vice-Chancellor for Research at the University of Illinois at Urbana-Champaign, where he is involved with the technical assessment and commercial licensing of intellectual property, and management of industry sponsored research.

Dr. Goss is a member of the Acoustical Society of America, the American Institute of Ultrasound in Medicine, the North American Hyperthermia Society, and Sigma Xi.

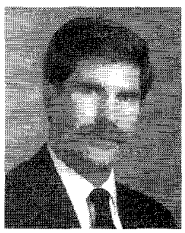

Leon A. Frizzell (S'71–M'74–SM'82) was born in West Stewartstown, NH, on September 12, 1947. He received the B.S. degree in physics from the University of New Hampshire, Durham, in 1969, and the M.S. and Ph.D. degrees in electrical engineering from the University of Rochester, Rochester, NY, in 1971 and 1976, respectively.

Since 1975, he has been in the Department of Electrical and Computer Engineering at the University of Illinois at Urbana-Champaign, where he is currently a Professor of Electrical and Computer Engineering and of Bioengineering. He has served as Chair of the Bioengineering Faculty since August 1995. His research interests are in ultrasound and include tissue characterization, biological effects, hyperthermia, surgery, and bioengineering.

Dr. Frizzell is a fellow of the American Institute of Ultrasound in Medicine, a fellow of the Acoustical Society of America, and a member of Eta Kappa Nu and Sigma Xi.

Jeffrey T. Kouzmanoff was born on October 14, 1963 in Urbana, IL. He received the B.S. degree in electrical engineering from the University of Illinois at Urbana-Champaign in 1986.

From 1982 to 1986 he served as a Technical Consultant and Computer Programmer to a number of firms, including DuoSoft Corporation, Savoy, IL; Electronic Courseware Systems, Savoy, IL; Rhino Robots, Champaign, IL; the University of Illinois, Department of Electron Microscopy, Urbana, IL; and the University of Illinois Computer Based Education Research Laboratory, Urbana, IL. In 1986, he joined Labthermics Technologies, Inc., Champaign, IL, where as Senior Research and Development Engineer, he is engaged in the design and development of software for hyperthermia and noninvasive focal ultrasound surgery control. His duties include software product design and development, software interface design for user control, and development of hyperthermia control algorithms for computer control.

Joseph M. Barich, a native of Chicago, IL, was born in 1972. He earned the B.S. and M.S. degrees in electrical engineering at the University of Illinois at Urbana-Champaign in 1994 and 1996, respectively. Since the fall of 1995 he has been a student at Boston College Law School pursuing his interest in patent and technological law.

Jeffrey M. Yang was born in Taiwan, R.O.C., on December 23, 1971. He received the B.S. degree in electrical engineering at the University of Illinois at Urbana-Champaign in 1994. He is currently working toward the M.S. degree in the Bioacoustics Research Laboratory of the University of Illinois.